ELSEVIER

Materials Science and Engineering A216 (1996) 193–200

MATERIALS SCIENCE & ENGINEERING A

Oxidation behavior of equiatomic TiNi alloy in high temperature air environment

C.L. Chu, S.K. Wu*, Y.C. Yen

Institute of Materials Science and Engineering, National Taiwan University, Taipei, Taiwan 106, Republic of China

Received 24 February 1995; revised 6 May 1996

Abstract

The isothermal oxidation behavior of equiatomic TiNi shape memory alloy in dry air from 550 to 1000°C is studied with thermogravimetric analysis. The alloy's scale layer is further investigated by X-ray diffraction (XRD), scanning electron microscopy (SEM) and electron probe microanalyzer. Experimental results indicate that a multi-layered scale is formed, consisting of an outer rutile layer, a porous intermediate layer of mixture of TiO_2 and Ni(Ti), and a thin inner $TiNi_3$ layer. The intermediate layer, furthermore, exhibits a stripe-like lamellar structure at the $TiNi_3$ interface. The apparent activation energy of TiNi alloy oxidation is 226 kJ/mol, and the oxidation rate follows a parabolic law. A schematic oxidation mechanism of TiNi alloy is proposed to explain the observed results.

Keywords: Isothermal oxidation test; TiNi alloy; Oxidation kinetics

1. Introduction

Among the many shape memory alloys (SMAs), equiatomic TiNi alloy is one of the most popular SMAs because it can be deformed in a ductile manner to more than 50% strain prior to fracture and shows a shape memory effect or pseudoelasticity at up to 8% strain [1]. In recent years, it has been used frequently as an industrial material and has many biomedical applications because of its unique properties [2] and good corrosion resistance [3]. However, as its applications are becoming widespread, more needs to be known about its chemical and mechanical properties, among these being the high temperature oxidation behavior in an air environment.

Titanium alloys are quite active and tend to react vigorously with oxygen to form oxides in air at elevated temperature. The thickness and structure of the oxided TiNi layer also play a significant role during the TiNi wire drawing processes [4], but to the best of our knowledge, there is little data on the oxidation behavior of TiNi alloys [5,6]. The mechanism of oxidation in TiNi alloys is also not very well understood. The purpose of this paper is to study the oxidation behavior of equiatomic TiNi alloy in a temperature range from 550 to 1000°C. The oxidation mechanism of this alloy is also discussed.

2. Experimental procedure

A conventional tungsten arc melting technique was used to prepare the equiatomic TiNi alloy. Titanium (purity, 99.7%) and nickel (purity 99.9%), totaling approximately 250 g, were melted and remelted at least six times in a low pressure argon atmosphere. Pure titanium buttons were also melted and used as getters. The mass loss during melting was negligible. The as-melted TiNi button was then hot-rolled at 850°C to a thickness of 3 mm. Specimens of $3 \times 3 \times 1$ mm for thermo-gravimetric analysis (TGA) and specimens of $10 \times 5 \times 3$ mm for isothermal oxidation testing were carefully cut from the hot-rolled sheet with a low-speed diamond saw. The cut specimens were polished on emery paper up to 1000 grit, then degreased ultrasonically in an acetone solution and weighed before the test.

A Du Pont Thermal Analysis Systems 9000 equipped with a TGA 51 thermogravimetric analyzer was used to run TGA analysis. The specimen was held in a plat-

* Corresponding author.

inum basket and surrounded by dry air flowing at a rate of 60 cm^3/min. Testing temperatures were between 700 and 1000°C. Each sample was heated from room temperature to the testing temperature at a rate of 100°C/min and then kept isothermally at that temperature for 20 min to 6 h.

In order to observe oxide structures, isothermal oxidation tests were also conducted in a furance with static air at temperatures between 550 and 1000°C. The testing time varied from 20 min to 6 h. After the oxidation period, the weight change of each sample was measured. Structures of TiNi specimens before and after oxidation were examined by X-ray diffraction (XRD). Cross sections of the oxided specimens were also examined by a Philips 515 SEM + EDAX and by a JEOL JXA-8600SX Electron Probe Microanalyzer (EPMA).

3. Results

3.1. Mass gain after the isothermal oxidation test

Fig. 1(a) shows the typical weight gain per unit surface area versus the exposure times in the flowing dry-air at 700 ~ 1000°C. Fig. 1(b) is the parabolic kinetics plot of the samples from Fig. 1(a). The weight gains at 700 and 775°C are rather small during the exposure period, but the weight gain increases rapidly at 1000°C. It is clear from Fig. 1(b) that the weight gain curves closely follow a parabolic law, despite the small deviation for the 1000°C curve. This indicates that the isothermal oxidation rate is a diffusion-controlled one. The reason for the small deviation in the 1000°C curve will be discussed in Section 4.2. Fig. 2 shows the Arrhenius plot for the parabolic rate constant. The apparent activation energy for the oxidation reaction of equiatomic TiNi alloy is determined to be 226 kJ/mol.

3.2. XRD of the oxidized surface

Fig. 3(a)–(e) show XRD patterns of equiatomic TiNi alloy before and after 60 min oxidation testing at 550, 700, 850 and 1000°C, respectively. Fig. 3(a) indicates the specimen consists of parent B2 phase and martensite B19′ monoclinic phase before the oxidation. White oxide layer is formed on the surface after the oxidation and, as revealed by XRD, the predominant constituent of this layer is TiO_2(rutile) for all the specimens of Fig. 3(b)–(e). Noted $TiNi_3$ peaks are observed for tests run at 550, 700 and 850°C. But these peaks disappear when the temperature rises up to 1000°C, as shown in Fig. 3(e). It is also found that there are no $TiNi_3$ peaks on the specimens' surface oxided at 1000°C for various exposure times. The reasons for this feature will be discussed in Section 4.1 of this paper. For the 850 and 1000°C oxidation tests of Fig. 3(d) and (e), respectively, "Ni" peaks are observed in the XRD patterns. From the Ti–Ni binary phase diagram [7], Ti can form a solid solution in f.c.c. Ni. Thus, we suggest that these "Ni" peaks do not represent pure Ni metal, but rather a phase of Ti atoms solid-soluted in Ni. We refer to this phase as Ni(Ti). The peak intensities of TiO_2 and Ni(Ti) become stronger as the oxidation temperature increases, as can be seen in Fig. 3(d) and (e).

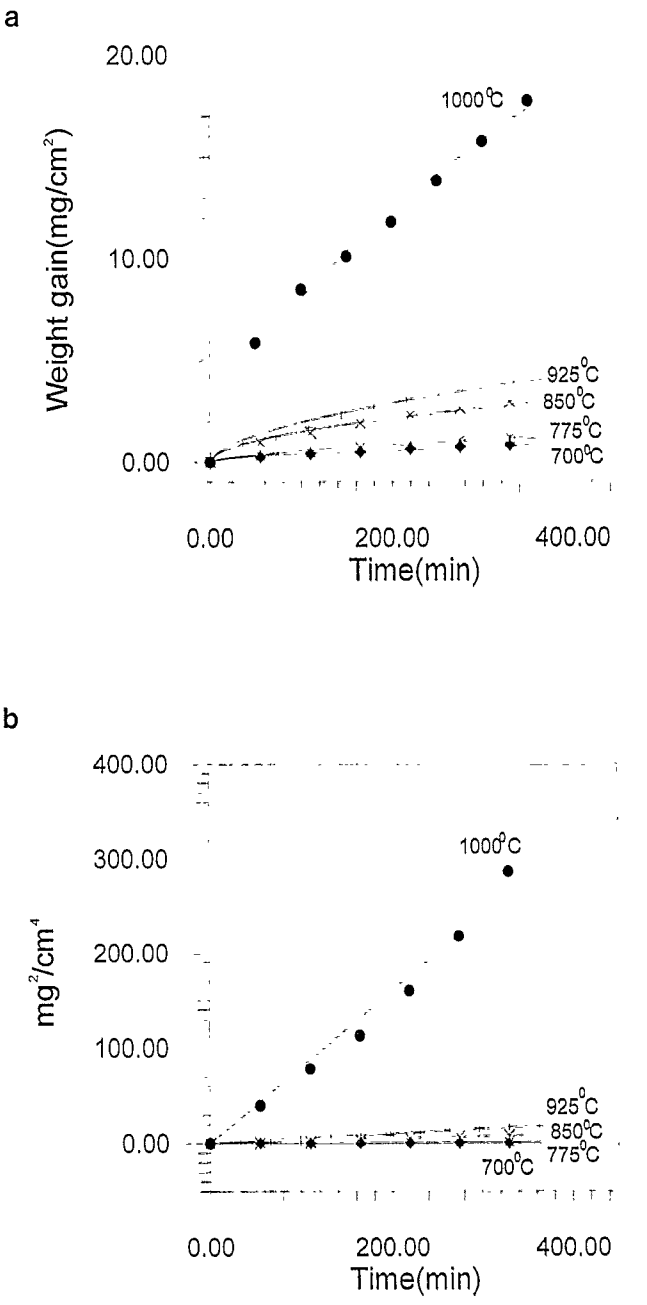

Fig. 1. Oxidation curves of the equiatomic TiNi alloy at temperatures from 700 to 1000°C. (a) Weight gain plot and (b) parabolic kinetic plot.

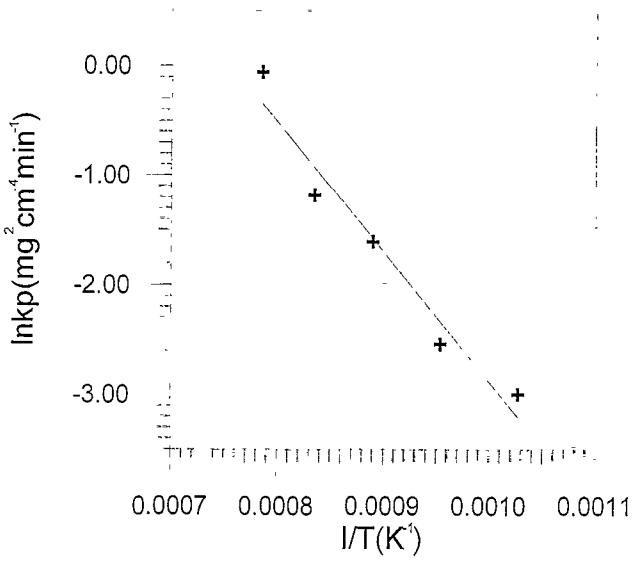

Fig. 2. Parabolic plots of the oxidation of equiatomic TiNi alloy.

3.3. Cross section observations of oxidized specimens

Typical cross sections of oxide scales observed in equiatomic TiNi alloy oxidized at 1000°C for various time intervals are shown in Figs. 4 and 5. Fig. 4(a)–(d) are scanning electron microscopy (SEM) photographs of specimens oxidized at 1000°C for 20 min, 40 min, 80 min and 6 h, respectively. Fig. 5(a)–(c) are the EPMA intensity line scan and the corresponding element mapping of Fig. 4(a)–(c), respectively. From Fig. 4, it is obvious that the oxide scale thickness is dependent on the time exposed. EDX results show that the oxide scale consists of three layers. The outer layer (layer I) consists mainly of rutile. The intermediate layer (layer II) consists of a mixture of rutile and Ni(Ti). While the third layer (layer III) is a relatively thin layer of $TiNi_3$. There is a distinct sublayer in layer II in the specimen oxidized for long periods of time, such as that shown in Fig. 4(d). Fig. 6 shows the thickness change of each oxide layer versus time for specimens of Fig. 4. It is obvious that layers I and II grow more rapidly than layer III. When the oxidation time exceeds 60 min, the growth of layer II is obviously faster than that of layer I.

The SEM micrographs of Fig. 4 show several large voids in layer I near the interface between layer I and II. On the other hand, layer II contains many small voids and/or uniformly distributed pores. The structure near the interface of layer II/III is a lamellar one. This lamellar structure is more obvious at higher temperatures and longer oxidation periods, as shown in Fig. 4(d), and is similar to that occurs in the oxi-

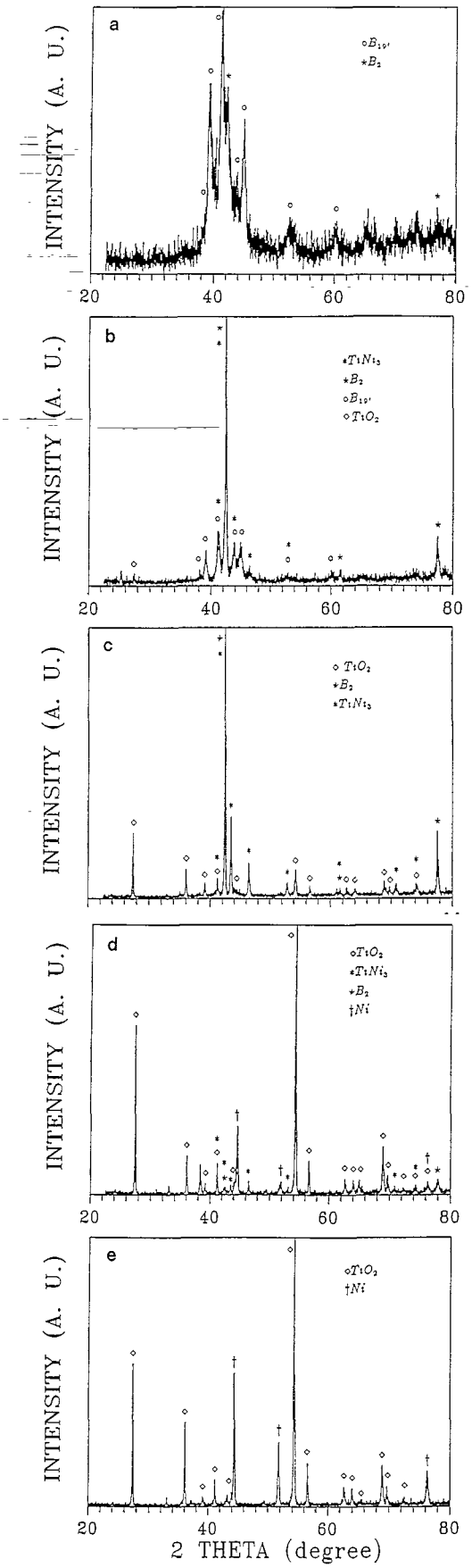

Fig. 3. XRD patterns of equiatomic TiNi alloy (a) before oxidation, and (b)–(e) after oxidation for 60 min at (b)550°C, (c)700°C, (d)850°C, (e)1000°C.

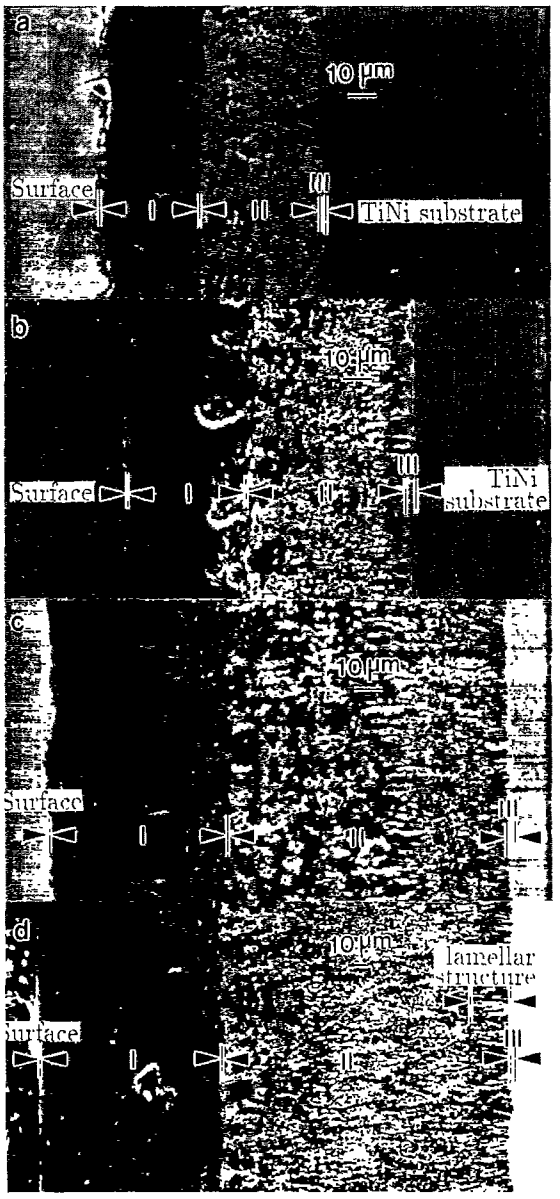

Fig. 4. SEM micrographs of cross-sections of equiatomic TiNi alloy oxidation at 1000°C for (a) 20min (b) 40min (c) 80min (d) 6h.

dation layer of binary TiAl intermetallic alloy [8,9]. The lamellar structure grow as stringers perpendicular to the layer II/III interface. EDX analysis shows that the white stripe of the lamellar structure is rich in Ni, while gray stripe is very rich in Ti, implying that the former is Ni(Ti) and the latter is rutile. This microstructure suggests that the layer II (mixture of TiO_2 and Ni(Ti)) is grown from the third $TiNi_3$ layer. Therefore, the oxide morphology in layer III may affect the oxidation behavior and influence the oxide morphology of layer II. The lamellar structure in layer II becomes indistinct as the distance from the layer II/III interface increases. At the same time, the development of pores becomes noticeable as this outward distance is increased.

4. Discussion

4.1. The oxidation mechanism of TiNi alloy

According to the experimental results mentioned above, a schematic diagram of the oxidation mechanism of TiNi binary alloy is proposed and shown in Fig. 7. Note that there is no NiO oxide formed in the scale in spite of the fact that TiNi contains a large amount of Ni. This may reflect the difference in the oxygen affinity between Ti and Ni, i.e., Ti is easily oxidized while Ni is more difficult to oxidize. Therefore, in the early stage of oxidation Ti is oxidized first to form oxides while Ni remains unchanged, as illustrated in stage 1 of Fig. 7. As the Ti oxide is formed becoming a continuous outer oxide scale on the specimen, the high temperature environment converts all the transient Ti oxides, TiO and Ti_2O_3, to the more stable oxide of rutile, TiO_2. This behavior was also proposed during the early oxidation stages of TiAl intermetallic alloy in a pure oxygen environment [8]. As the rutile crystals grow, both in the vertical and horizontal directions, a rutile enriched layer is formed. This leads to a local enrichment of Ni just beneath the TiO_2 layer, as shown in stage 2 of Fig. 7. As the oxidation progresses, titanium atoms diffuse outward while oxygen atoms diffuse inward. The diffusivity of Ti in rutile is faster than that of oxygen [10], whereas Ni appears to follow a Kirkendall effect for its interdiffusion with Ti. This results in an outward growth of rutile and an inward growth of Ni-rich phases, such as Ni(Ti). Thus, we have a mixture layer of TiO_2 and Ni(Ti) beneath the TiO_2 layer, as shown in stage 3 of Fig. 7. As mentioned above, XRD results of Fig. 3(b)–(e) show that $TiNi_3$ peaks appear in oxide scales of specimens oxidized at 550, 700 and 850°C, but not in those oxidized at 1000°C. This may be due to the thickness of oxide scale which is greater than 0.05 mm for the 1000°C × 80 min oxidation, which may have prevented penetration by the X-ray beam and prevented the detection of $TiNi_3$ phase. Another possibility is that the high diffusivity of Ti and O atoms at 1000°C makes the $TiNi_3$ phase unstable, i.e., the TiNi oxided at 1000°C decomposes to TiO_2 and Ni(Ti) directly instead of TiO_2 and $TiNi_3$.

The formation of large voids near the interface between the rutile (layer I) and beneath layer II can be explained in terms of the growth of rutile crystals. During the initial stages of formation, rutile grows almost normal to the specimen surface. Later, lateral growth predominates. The lateral growth continues until the rutile crystals meet each other. Then, sintering takes place due to the high temperature. The large voids are possibly formed due to the difference between the vertical and lateral growth rates. This feature is illustrated in stage 3 of Fig. 7.

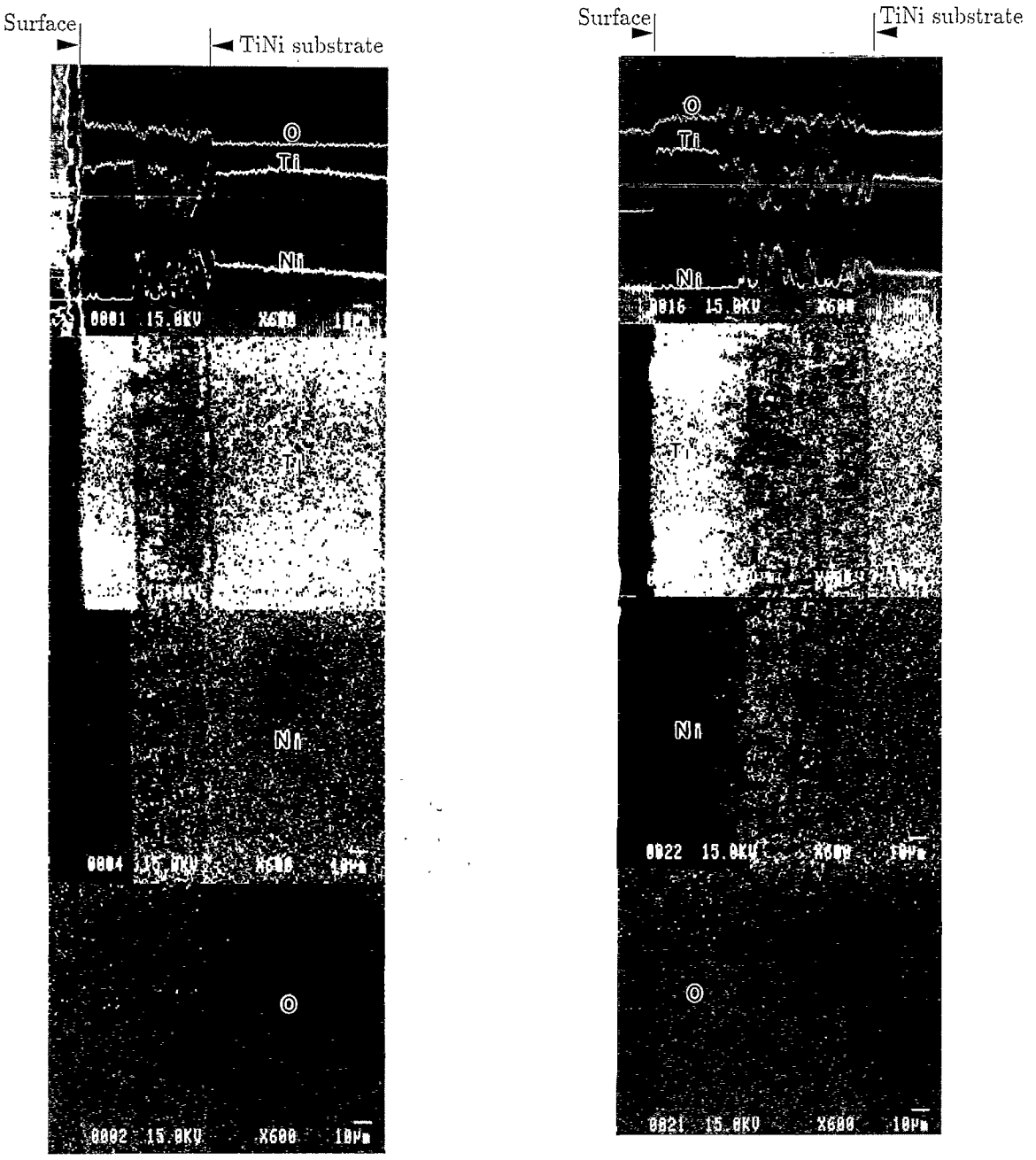

Fig. 5. (a) EPMA line scan and elements Ti, Ni and O mappings of Fig. 4(a). (b) EPMA line scan and elements Ti, Ni and O mappings of Fig. 4(b). (c) EPMA line scan and elements Ti, Ni and O mappings of Fig. 4(c).

While the outer layer (layer I) of TiO_2 and the intermediate layer (layer II) of TiO_2 and Ni(Ti) become thicker and thicker, a Ti depletion layer (layer III) is formed at the layer II/layer III interface due to the outward diffusion of Ti from the metal. This leads to the formation of a $TiNi_3$ phase in this Ti-depleted layer, as shown in stage 4 of Fig. 7. At the same time, a sublayer of lamellar morphology near the layer II/III interface, as illustrated in Fig. 4(d), is formed due to the interdiffusion of Ti and Ni in which titanium diffuses outward while nickel diffuses inward. We suggest that the formation of pores in this sublayer is closely related to the Kirkendall effect of Ti and Ni interdiffusion in which vacancies may collect to form cavities and pores at the metal/scale interface and produce appreciable porosity in the scale after more extended reaction.

4.2. The oxidation kinetics of TiNi alloy

The apparent activation energy for the equiatomic TiNi alloy derived from this study is compared with that of reported data for TiNi alloys [5] and for titanium, rutile and alumina which was prepared by Welsch and Kahveci [11], as listed in Table 1. The

oxidation resistance of equiatomic TiNi alloy is near that of pure Ti and superior to that of low aluminum content Ti alloys, but lower than that of titanium aluminides with Al $\geqslant$ 25 at.%. At the same time, the activation energy of oxidation in TiNi alloy is close to that of oxygen diffusion in rutile but less than that of oxygen diffusion in alumina. These data are consistent with our observations that the oxidation of TiNi alloy is mainly characterized by the rutile formation with nickel oxidation being absent.

During the intial periods of oxidation, mass gain is mainly due to the growth of rutile which is the main component of the outer oxide layer. Once the TiO_2 oxide layer reaches a certain thickness, the Ti diffusion distance increases. Meanwhile, as mentioned above, the result of activation energy of oxidation in TiNi alloy indicates that the oxygen diffusion in TiO_2 oxide layer is predominant. This suggests that the main growth direction of the scale layer becomes inward. From Fig. 6, one can find that layers I and II show a parabolic growth during the oxidation period of 1000°C × 20 ~ 360 min. This phenomenon would lead us to expect

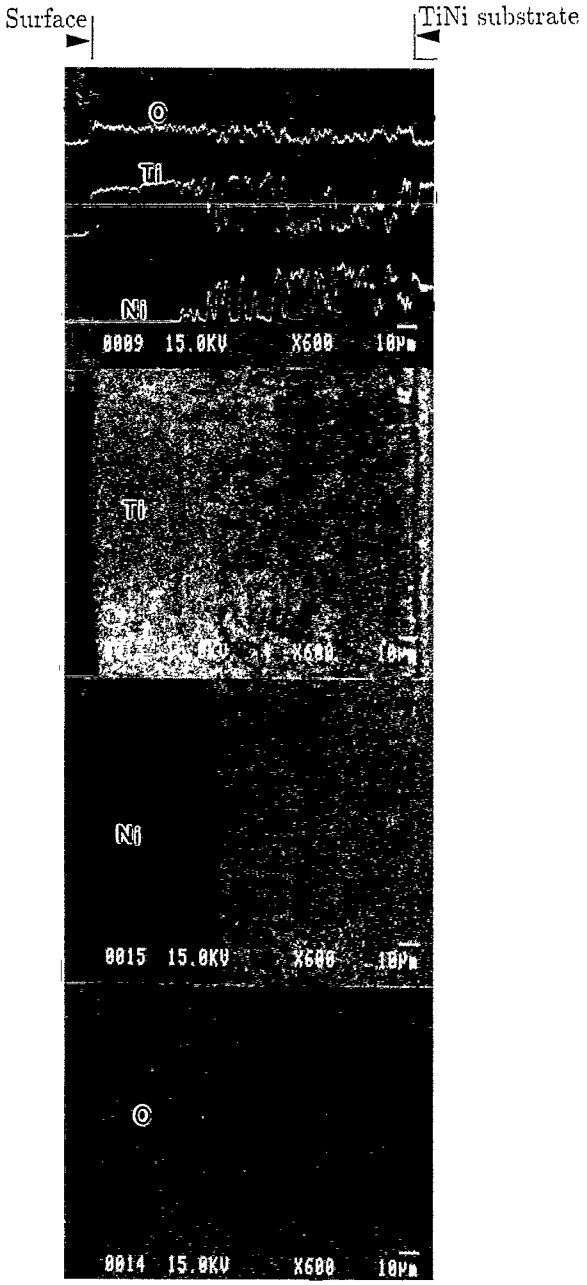

Fig. 5 (C)

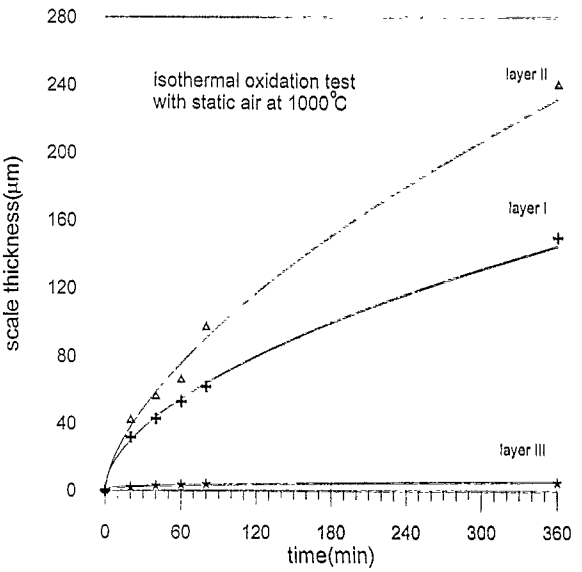

Fig. 6. Thickness change of each oxide layer versus time in the oxided scale of Fig. 4.

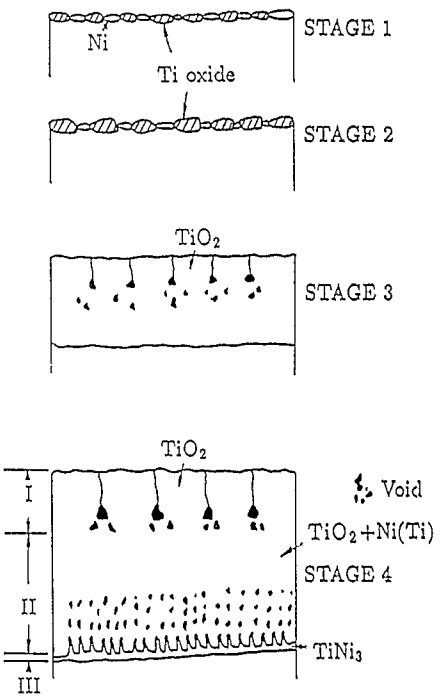

Fig. 7. Schematic diagram of oxidation scale formation of equiatomic TiNi alloy.

Table 1
Activation energy data of oxidation and diffusion in pure Ti, Ti alloys, rutile, alumina, titanium aluminides, Ni_3Al alloy and TiNi alloy

	Reference[a]	Q, kJ/mol
Oxidation of Ti	[14]	265
Oxidation of Ti	[15]	239
Oxidation of Ti	[16]	235
Oxidation of Ti–2.6at.%Al	[15]	183
Oxidation of Ti–16at.%Al	[15]	209
Oxidation of Ti–25at.%Al	[17]	269
Oxidation of Ti–26at.%Al	[17]	255
Oxidation of Ti–34at.%Al	[17]	299
Oxidation of Ti–49at.%Al	[17]	419
Oxidation of Ti–50at.%Al	[17]	423
O-diffusion in rutile	[18,19]	251
O-diffusion in rutile	[16]	234
Ti-diffusion in rutile	[20]	257
O-diffusion in alumina	[21]	460
Oxidation of Ni–25at.%Al	[22]	286
Oxidation of TiNi (equiatomic)	[this work][b]	226
Oxidation of TiNi	[5][c]	247

[a] Original table was prepared by Welsch and Kahveci, Ref. [11].
[b] TiNi alloy was oxided at 700~1000°C for up to 6 h.
[c] TiNi alloy was oxided at 750~950°C, Ref. [5].

that the oxidation rate follows a parabolic rate law. However, the data of layer II shown in Fig. 6 have small deviation from the parabolic curve for an exposure time greater than 60 min. We believe that this small deviation is closely related to the voids/pores formed in layers I and II. Voids/pores, such as those occurring in samples oxidized at 1000°C × 60 min and 6 h of Fig. 4(c) and (d) respectively, can enhance oxygen diffusion and thus cause small deviation in the oxidation rate from the parabolic law. The deviation of the 1000°C parabolic curve of Fig. 1 can also be explained by the same argument.

4.3. The B2 and B19′ phases in TiNi alloy

From Fig. 3(a), the alloy used in this study contains parent B2 (CsCl) phase and martensite B19′ phase at room temperature. Obviously, the M_s point (the starting temperature of martensitic transformation) of TiNi alloy used in this study is above room temperature while the M_f (the finishing temperature of martensitic transformation) is below room temperature. Before oxidation, the intensity peak of B19′ is higher than that of B2. However, as shown in Fig. 3(b), the intensity peak of B2 phase is higher than that of B19′ after oxidation at 550°C. This feature indicates that the M_s and M_f points of TiNi sample near the oxide scale are suppressed and the volume fraction of B2 phase is increased at room temperature. Only peaks of B2 phase appear in the XRD patterns of 700 and 850°C oxidized specimens. This indicates that the M_s point has been suppressed to a temperature below room temperature. In samples oxidized at 1000°C, there is no B2 peak in XRD pattern. This may be due to the thickness of the oxide scale which prevents detection. In all, the suppression of M_s and M_f points can be explained by the absorption of interstitial oxygen atoms in the TiNi lattice during the oxidation [12]. These interstitial oxygen atoms can suppress the M_s point in TiNi alloy [13].

5. Conclusions

The study of oxidation behavior of equiatomic TiNi alloy leads to the following important conclusions.

(1) The apparent activation energy of equiatomic TiNi SMA obtained in this study is 226 kJ/mol which is higher than that of Ti alloy containing low levels of aluminum but lower than that of titanium aluminides with Al ⩾ 25 at.%.
(2) The scale consists of three layers: an outer rutile layer, an inner thin and nickel rich layer $TiNi_3$, and a porous intermediate layer consisting of a mixture of rutile and Ni(Ti).
(3) Oxidation at temperatures between 550 and 1000°C in dry air follows approximately parabolic laws. The oxidation rate may deviate from the parabolic curve due to voids/pores developed in the scale of specimens oxidized at 1000°C for an exposure time longer than 60 min.
(4) A stripe-like lamellar structure forms in the intermediate oxide layer and near the thin $TiNi_3$ layer. The lamellae themselves have metal/oxide interfaces and are attributed to the interdiffusion of Ti and Ni between layers II and III.
(5) The M_s and M_f points of the substrate TiNi alloy near the oxide scale are suppressed after the alloy oxidized at temperatures above 550°C. The interstitial oxygen absorbed in the TiNi lattice are believed to cause this phenomenon.

Acknowledgements

The authors are grateful to Mr Shyh-Wei Wu, graduate student of Material Science and Engineering, National Taiwan University for his kind help in part of the experimental work. We are also pleased to acknowledge the financial support of this research by National Science Council (NSC), Republic of China, under Grant No. NSC 83-0405-E002-029.

References

[1] S. Miyazaki, K. Otsuka, and Y. Suzuki, *Scr. Metall.*, *15* (1981) 287.

[2] D.E. Hodgson, M.H. Wu and R.J. Biermann, Shape memory alloys, *Metals Handbook*, ASM, 10th edn., Vol. 2, 1991, pp. 897–902.
[3] R.S. Ruta, A.S. Gadiyar, K. Madangopal and S. Baneriee, *Corrosion, 28* (3) (1993) 217.
[4] S.K. Wu, H.C. Lin and Y.C. Yen, *Mater. Sci. Eng., A*215 (1996) 113.
[5] T. Satow, T. Isano and T. Honma, *J. Jpn. Inst. Met., 38* (1974) 242 (in Japanese).
[6] M.T. Yeh, M.J. Chiou and H.P. Kao, *Proc. Annu. Conf. Chinese Society for Material Science, Taiwan, Vol. 1, 1993*, p. 179 (in Chinese).
[7] *Metal Handbook, Alloy Phase Diagram*, ASM International, USA, Vol. 3, 1992, pp. 2–319.
[8] S. Taniguchi, T. Shibata and S. Itoh, *Mater. Trans. JIM, 32* (2) (1991) 151.
[9] Y. Shida and H. Anada, *Mater. Trans. JIM, 34* (3) (1993) 236.
[10] S.A. Kekare, D.K. Shelton and P.B. Aswath, *Oxidation of High-Temperature Intermetallics*, The Minerals, Metals & Materials Society, Warrendale, PA, 1993, p. 325.
[11] G. Welsch and A.I. Kahveci, *Oxidation of High-Temperature Intermetallics*, The Minerals, Metals & Materials Society, Warrendale, PA, 1989, p. 207.
[12] S.K. Wu and C.M. Wayman, *Acta Metall., 36* (1988) 1005.
[13] H. Funakubo (ed.), *Shape Memory Alloys*, University of Tokyo, 1984, pp. 98–99.
[14] W.W. Smeltzer, R.R. Haerig and J.S. Kirkaldy, *Acta Metall., 9* (1961) 880.
[15] A.M. Chaze, C. Coddet and G. Beranger, *J. Less-Common Met., 83* (1982) 49.
[16] J. Unnam, R.N. Shenoy and R.K. Clark, *Oxid. Met., 26* (1986) 231.
[17] N.S. Choudhury, H.C. Graham and J.W. Hinze, in Z.A. Foroulis and F.S. Pettit (eds.), *Proc. Symp. Properties of High Temperature Alloys*, Electrochem. Soc. Proc., Vol. 77–1, 1976, p. 668.
[18] P. Kofstad, *Nonstoichiometry, Diffusion, and Electrical Conductivity in Binary Metal Oxides*, R.E. Krieger, Malabar, FL, 1983, pp. 142–149.
[19] R. Haul and G. Dumbgen, *J. Phys. Chem. Sol.* (1961) 1.
[20] L. Venkatu and L.E. Potet, *Mater. Sci. Eng., 5* (1969/70) 258.
[21] Y. Oishi and W. D. Kingery, *J. Chem. Phys., 33* (1960) 905.
[22] F.S. Pettit, *Trans. TMS-AIME, 239* (1967) 1296.